THE ATLANTIC-WIDE RESEARCH PROGRAMME FOR BFT (GBYP Phase 14)

SHORT-TERM CONTRACT (ICCAT GBYP Phase 14)

Design-based inference to estimate density, abundance, and biomass of Bluefin Tuna in the Mediterranean Sea: analysis including the aerial visual surveys from 2017 to 2024.

FINAL REPORT

December 2024

CREEM, University of St Andrews

L. Burt, M. Chudzińska, C. G. M. Paxton

Please cite this report as: Burt *et al*. (2024). Design- based inference to estimate density, abundance, and biomass of bluefin tuna in the Mediterranean Sea: analysis including the aerial visual surveys from 2017 to 2024. Report number CREEM-2024-08. Provided to ICCAT, December 2024 (Unpublished).

Document control

Please consider this document as uncontrolled copy when printed.

Version	Date	Reason for issue	Prepared by	Checked by
1	17 December 2024	First draft	LB	MC, CP
2	19 December 2024	Draft submission to ICCAT	LB	
3	20 December 2024	Final report	LB	

CREEM
Centre for Research into Ecological and Environmental Modelling

University of St Andrews

1 Contents

2 Summary

Data from aerial surveys that took place in summer 2024 in three regions (A, C and E) in the Mediterranean Sea have been combined with data from surveys in previous years (2017-2023) to provide an update of estimates of abundance and biomass of Bluefin tuna. Line transect distance sampling methods were employed on the surveys and in 2024, 17,910 km of search effort were flown, and 18 groups of non-juvenile Bluefin tuna were detected on search effort. Various subsets of the data are used to obtain abundance of individuals and total biomass. Using survey data from four regions (A, C, E and G) and years 2017 to 2024, abundance for 2024 was estimated to be 11,335 fish (CV=0.7), 30,890 fish (CV=0.7) and 105,260 fish (CV=0.5) in regions A, C and E, respectively. Biomass was estimated to be 2,200 tonnes (CV=0.8), 3,907 tonnes (CV=0.7) and 9,772 tonnes (CV=0.6) in regions A, C and E, respectively.

3 Introduction

Aerial surveys have been undertaken in Mediterranean Sea to detect Bluefin tuna (BFT) from 2010 to 2024 under the auspices of the International Commission of the Conservation of Atlantic Tunas (ICCAT) Atlantic-wide research programme for Bluefin Tuna (GBYP). The main objectives of this programme are to improve a) understanding of the key biological and ecological processes, b) current assessment methodology, c) management procedures and d) advice. This report presents the data collected during the visual aerial survey data in 2024 and presents estimates of density, abundance and biomass estimates of BFT in the Mediterranean Sea in the three surveyed regions, or blocks, (A, C and E) and updates the indices in previous reports (e.g. Chudzinska et al 2023) using the survey data collected from 2017.

Estimates are obtained using line transect distance sampling methods (Buckland et al. 2001) and the tuna indices are updated in two ways: revision (referred to as actualisation in previous reports) of estimates (Task 1), and strict update (Task 2). These are described below.

3.1.1 Task 1: Revision of the tuna indices

Paxton et al. (2023) estimated density, biomass and abundance (referred to as 'indices') of BFT for the Mediterranean Sea survey blocks for years 2017-2022 and compared them to the estimates from the previous analysis (Chudzinska et al. 2021, Chudzinska et al. 2022). Although aerial surveys in region G (southern coast of Turkey) of the Mediterranean Sea stopped being conducted in 2019, including these data results in different estimates compared to excluding these data from the analysis (Chudzinska et al. 2023). Indeed, adding more data has the potential to change estimates.

In Task 1, the aerial survey data collected in 2024 (in blocks A, C and E) were added to data collected in years 2017-2023. Line transect distance sampling methods (Buckland et al. 2001) were used to estimate density, abundance and biomass for blocks A, C and E for the years 2017- 2024. In addition, we included data from block G (collected in years 2017-2019) and obtained estimates for 2017-2024 for blocks A, C and E.

3.1.2 Task 2: Strict update of the tuna indices

Building a detection function based on an updated data set (e.g. additional years of data), may result in different covariates (explanatory variables) being retained in the final model compared to a model estimated without the additional data. Alternatively, it may result in the same covariates being retained in the final model but the values of the coefficients for these covariates will differ compared to the model with the same covariates but based on reduced data set. Consequently, a detection function based on the updated data set may result in different estimates of tuna indices compared to indices for previous years obtained without the additional data.

To provide a strict update, the detection function fitted in Paxton et al. (2023) (i.e. the same variables and values of the model parameters) were used to obtain alternative estimates for 2024 abundance and biomass respectively. This approach was taken in Chudzinska et al. (2024).

4 Methods

4.1 Overview of the aerial surveys

Three blocks, A, C and E were surveyed in 2024 (Figure 1). Details on survey protocols and outcomes are provided by Popov and Feron (2024) and Unimar and AerialBanners (2024a, 2024b), and so here we provide only information relevant for this report.

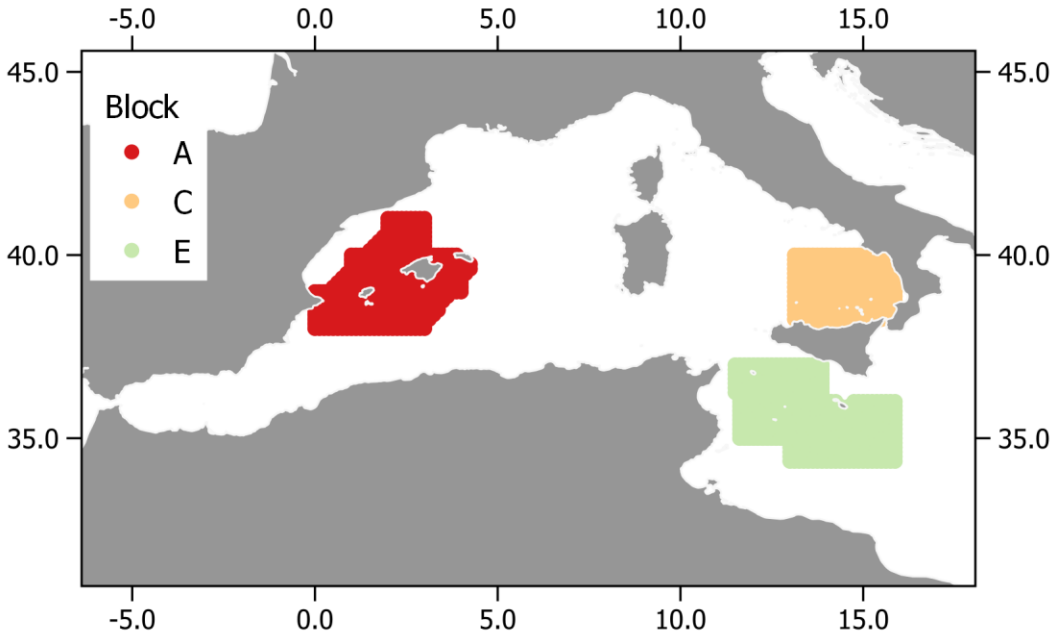

Figure 1. Depiction of Mediterranean Sea and the three survey blocks.

Table 1 summarises the timing, company and airplane type used for surveys in 2024. These surveys were conducted by the same companies and using the same type of aircrafts as recent surveys (Appendix A).

Table 1. Summary of the survey blocks in 2024.

Block	Dates	Company	Airplane
A	04 June – 24 June	Air Perigord	Cessna
C	04 June – 06 July	Unimar/Aerial Banners	Partenavia
E	11 June – 01 July	Unimar/Aerial Banners	Partenavia

4.2 Statistical methods

Line transect distance sampling methods (Buckland et al. 2001) were used to estimate density and abundance and these methods are described below.

4.2.1 Estimating density and abundance

In distance sampling (DS) methodology, the perpendicular distances to detections of BFT are used to model how detectability decreased with increasing distance, and hence estimate a probability of detection ($\hat{p}$). Using standard methodology (Buckland *et al*. 2001), the estimated density ($\widehat{D}$) and abundance ($\widehat{N}$) of fish in a survey block was obtained from

$$\widehat{D} = \frac{n}{2wL}.\frac{1}{\hat{p}}.E[s]$$

$$\widehat{N} = A.\widehat{D}$$

where for each block, A is the size of the block, n is the number of detected schools, w is the truncation distance associated with the detection function, L is the total length of transects covered on search effort and $E[s]$ is the expected school size.

Biomass of fish is also of interest and to obtain this, school size was replaced in the equation above by expected biomass (which has been recorded for each detected school).

In this standard approach, perpendicular distance is the only explanatory variable used to obtain $\hat{p}$ but the model can easily be extended to include additional explanatory variables which affect detectability, such as school size (Marques and Buckland, 2003).

As additional detections (years and/or regions) are included in the detection function, the probability of detection may change, hence altering the estimated densities in each year and region. For example, although aerial surveys in region G (southern coast of Turkey) stopped being conducted in 2019, including these detections in the detection function indices results in

different estimates compared to excluding these data from the analysis (Paxton *et al*., 2023). Here we propose two main tasks: Task 1) to use all data available to date to estimate the detection function (with and without region G) and hence update estimates for all years and blocks A, C and E, and Task 2) to avoid previous estimates being changed (because of including new data in the detection function) we use the detection function fitted by Paxton *et al*. (2023) to obtain a 'strict' update of density and abundance estimates. Further details are provided below.

4.2.2 Calculating perpendicular distance

As for previous surveys, the perpendicular distance from the detected school to the transect was calculated using the trigonometric relationship:

$$y_i = h_i * \tan((90 - \theta_i)$$

where y_i is the perpendicular distance between the transect and the i^{th} school, θ_i is the declination angle measured when the plane was a beam and h_i is the height of the airplane above sea level when abeam (Figure 2).

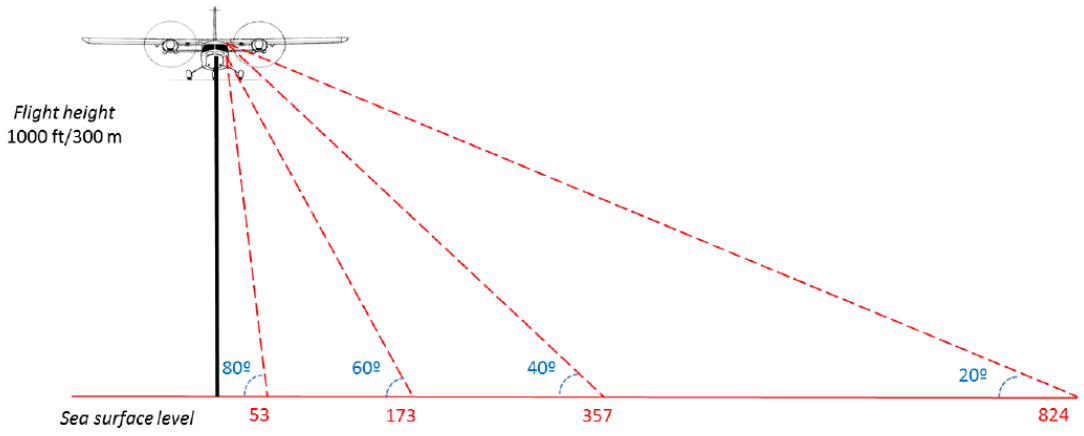

Figure 2. Example of the key declination angles and perpendicular distances at an altitude of *h* = 1000 ft = 300 m (Figure 5 from ICCAT survey protocol. Source: https://www.iccat.int/.)

4.2.3 Fitting the detection function

Two critical assumptions of DS methods are that all schools on the transect (i.e., at zero perpendicular distance) are detected with certainty and that distance measurements are exact (i.e., measured without error). Given these assumptions, the distribution of perpendicular distances is used to model how the probability of detection decreases with increasing distance from the transect. If detection on the transect is not certain (i.e. $g(0)<1$), the estimates will underestimate the true abundance and will represent estimates of relative numbers of animals.

Perpendicular distances were right truncated to 1500 m, to avoid a long tail in the detection function. The choice of this truncation distance was based on visual inspection of fitted detection function and comparison with truncation distance used for previous analyses (e.g.

Paxton et al. 2023). No left truncation was applied; left truncation is a common practice for aerial surveys, due to difficulties in searching directly underneath the plane, especially when the plane does not have a bubble window, however, the planes used in the aerial surveys under consideration in this report were fitted with bubble windows.

As in the analysis in the previous years, only sightings from professional observers were used and schools that were recorded as 100% small (i.e. individual fish < 25kg) were excluded.

The analysis was performed in R version 4.4.0 (R Core Team 2024) using the packages Distance (Miller et al. 2019) and mrds (Laake et al. 2020).

4.2.3.1 Task 1

Detection functions were selected using all years and blocks, and excluding area G and using school sizes or biomass; the detection functions are numbered as follows:

1A. detections from 2017-2024 from blocks A, C, E and G, using school size

1B. detections from 2017-2024 from blocks A, C, E and G, using biomass

1C. detections from 2017-2024 from blocks A, C and E using school size, and

1D. detections from 2017-2024 from blocks A, C and E, using biomass

In each case, two key functions, the half normal and the hazard-rate, were tried and whether adding explanatory variables (in addition to perpendicular distance) to the model in a multiple-covariate distance sampling (MCDS; e.g. Marques et al. 2007) approach would improve model fit. Here, five variables which may explain any differences in the detection of schools were considered (Table 2). The natural logarithm of the school size (and biomass) was used due to large variation in observed sizes and biomass (Figure). Appendix A contains the factor levels for each block used in this report.

Table 2. Covariates considered for multiple-covariate distance sampling analyses.

Covariate	Description
Log(size)	Log of school size or biomass
company	Factor with five levels (ActionAir, Airmed, Air Perigord, Unimar, Unimar/Aerial Banners)
airplane	Factor with two levels (Partenavia, Cessna)
year	Factor with seven levels (2017, 2018, 2019, 2021, 2022, 2023, 2024)
block	Factor with four levels (or three levels when block G is excluded)

Initially, models without any covariates (null models) were fitted. We then fitted single covariate models to both key functions using the five available covariates. Finally, models which included a combination of *log(size)* and each of the remaining variables were fitted. More complicated models (i.e. three additional covariates) were not considered because the factors are confounded (e.g. the companies always use the same type of plane). This process was consistent with model fitting conducted in the previous years (Paxton et al. 2023). Model

selection was based on minimum AIC values, but if a simpler model was within 2 AIC units of the minimum model, then the simpler model was selected (Akaike 1987).

To assess goodness of fit of the model, a quantile-quantile (Q-Q) plot and Cramer-von Mises tests (in function gof_ds) were obtained; a large *p*-value indicates an adequate fit of the model to the observed data (Miller et al. 2019, Laake et al. 2022).

4.2.3.2 Estimating density and abundance and biomass

Detections and search effort were pooled within each block and year to obtain encounter rates, and hence obtain estimates of density and abundance, by year for blocks A, C and E. The lengths of the realised transects were calculated from the recorded positions (i.e. latitude and longitude), when observers were on search effort.

The same approach was used to estimate biomass; in this case, the size of observed schools was replaced by the estimated biomass.

Schools that were recorded as 100% small schools (or all small fish <25 kg) were excluded. The remaining schools are referred to as adult schools.

4.2.3.3 Task 2

In Paxton et al. (2023), the variables selected in the detection function were *company* and *log(size)* to estimate tuna abundance and *company* and *log(biomass)* to estimate tuna biomass. These detections functions were fitted to data from 2017 to 2022 in blocks A, C, E and G. These models (i.e., using the same model parameter values) were applied to obtain estimates for 2023 (as in Chudzinska et al., 2024) and 2024. This means that detections from these years are not included in the detection functions. To avoid changing the parameters, we have applied the same levels of company used by Paxton et al (2023) to apply the detection function to the 2024 data.

5 Results

5.1 Summary of search effort, encounter rate and sightings for 2024 data

Table 3 summarises the search effort and sightings for the 2024 survey; the largest search effort per block was conducted in block E and lowest in block C. A similar number of schools were detected in blocks A and E. Figure 3 shows the locations of the search effort and detected schools.

Table 3. Summary of survey data in each block in 2024. The schools included were detected during search effort and represent adult schools. Note all schools were detected within 1,500m of the transects.

Block	Number of transects	Search effort (km)	Number of schools
A	30	5687.5	7
C	25	4988.3	3

E	34	7234.1	8

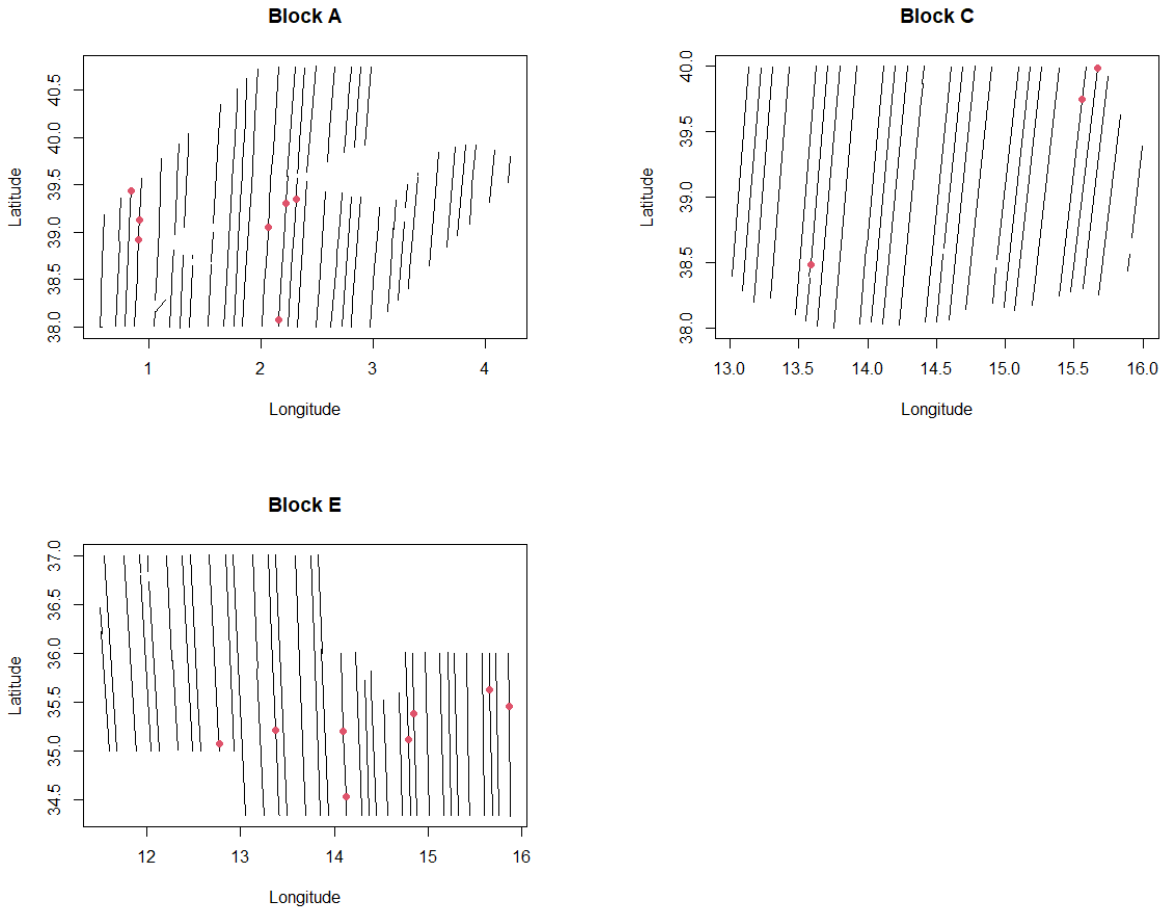

Figure 3. 2024 survey transects (grey lines) and detected schools (red dots) in the three blocks: A, C and E. The detections represent on-effort detections of adult schools before truncation.

The highest encounter rate occurred in block A and the lowest in block C (Table 4).

Table 4. Size of the area covered by the survey and number of adult schools encountered within 1,500 m (*n*), estimated encounter rate (ER; schools per km) and associated coefficient of variation (CV).

Block	Covered area (km^2)	*n*	ER	CV
A	17062.6	7	0.0036	0.43
C	14965.0	3	0.0006	0.55
E	21702.2	8	0.0011	0.37

The median school sizes observed in 2024 were smaller than recent years but like school sizes in years 2017 to 2019. This pattern was also reflected in the biomass (Figure 4).

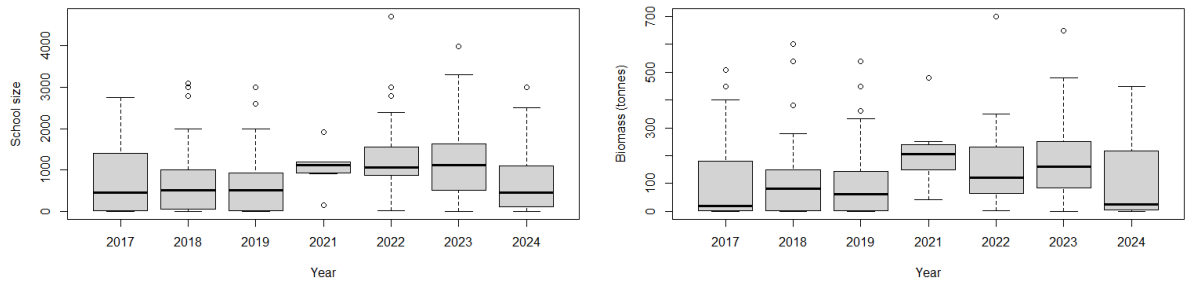

Figure 4. Distribution of observed adult school sizes (left) and their biomass (right) by year. The thick horizontal line indicates the median of the distribution and dots indicate values more than 1.5. times the interquartile range (height of the box) from the central box. Note 1000 kg = 1 tonne.

A summary of the data from previous years is given in Appendix A.

5.2 Task 1 –revision of indices based on data from four blocks (A, C, E and G)

5.2.1 Detection functions for abundance and biomass

The selected model for abundance included terms for logarithm of school *size* and *company* and the selected model for biomass included terms for logarithm of *biomass* and *company*. In both models a half-normal detection function was selected. See Appendix B (Table B1 and B2) for a full list of fitted models and goodness of fit of the selected models.

The histograms of perpendicular distances show fewer detections after 500 m and, not surprisingly, smaller schools (in number and weight) are detected at shorter distances (Figure 5).

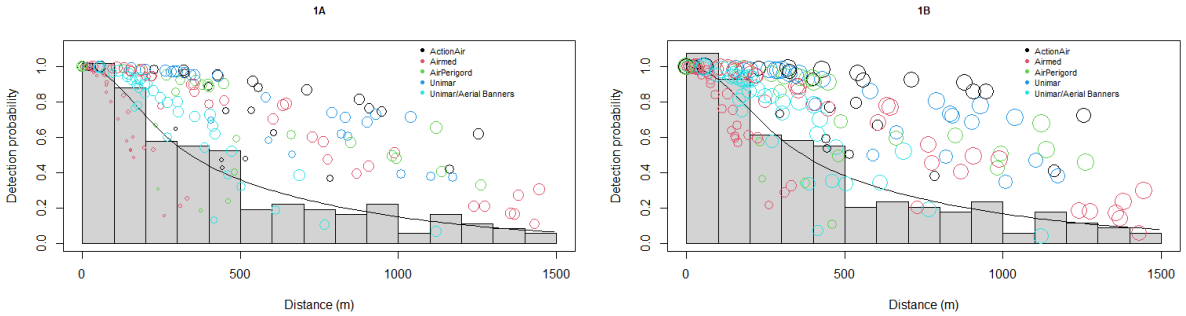

Figure 5. Detection functions 1A (abundance) and 1B (biomass): histogram of observed distances, detection function averaged across all observations (black line) and detection probabilities of observed distances from best fitting model colour coded by plane/company. Size of symbols are scaled to represent the logarithm of school size (1A) and logarithm of biomass (1B).

5.2.2 Estimated abundance for years 2017-2024

Estimated abundance of fish is given in Table 5. For block E, abundance was higher in recent years compared to the early surveys. This contrasts with block A where there is a decrease in

recent years. After a large increase in 2022 in block C, estimated abundance in 2023 and 2024 is like that in earlier years. Figure 6 shows a comparison between current estimates and estimates of the abundance from the Chudzinska et al. (2024); the current results are comparable with these previous estimates. Differences in 2022 are due to making minor corrections in the 2022 data.

Table 5. Estimated number of individual tuna (N, in thousands) per block and year with coefficient of variation (CV), and lower (LCL) and upper (UCL) 95% confidence levels. The orange values are from Chudzinska et al. (2024). All estimates are based on detections from all blocks: A, C, E and G.

Block-year	N	CV	LCI	UCI	N	CV	LCI	UCI
	This report				Chudzinska et al. (2024)			
A-2017	54.3	0.4	24.0	113.0	51.6	0.4	22.8	117.0
A-2018	88.9	0.3	49.7	158.9	84.4	0.3	47.0	151.5
A-2019	83.9	0.4	39.2	179.4	79.8	0.4	37.3	170.7
A-2021	30.2	0.5	10.9	83.9	29.3	0.5	10.6	80.8
A-2022	64.2	0.4	27.5	149.7	39.4	0.4	18.8	82.5
A-2023	59.8	0.5	24.2	147.9	59.7	0.5	24.1	147.6
A-2024	11.3	0.7	3.2	39.6				
C-2017	48.2	0.4	201.6	107.7	45.4	0.4	20.4	101.1
C-2018	40.0	0.6	13.4	119.5	37.7	0.6	12.7	112.4
C-2019	27.9	0.6	9.2	84.4	26.3	0.6	8.7	79.4
C-2022	178.5	0.4	82.3	387.2	158.4	0.4	71.2	352.5
C-2023	37.2	0.7	10.7	129.0	33.2	0.7	9.5	115.8
C-2024	30.9	0.7	8.9	106.7				
E-2017	49.8	0.5	18.7	132.5	45.5	0.5	17.1	121.1
E-2018	42.9	0.6	14.4	127.8	40.4	0.6	13.6	120.2
E-2019	20.5	0.5	8.3	50.8	19.0	0.5	7.7	46.8
E-2022	22.7	0.8	5.2	98.8	45.3	0.8	11.2	183.3
E-2023	167.4	0.4	77.1	363.3	149.4	0.4	67.0	333.2
E-2024	105.3	0.5	44.3	250.1				

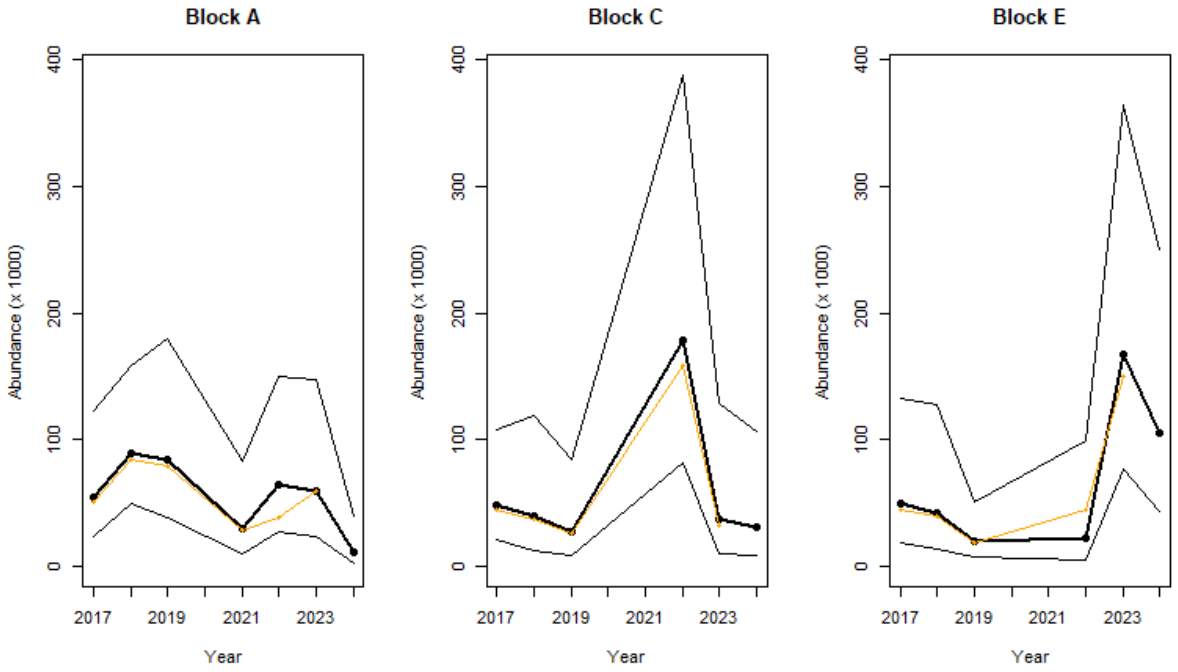

Figure 6. Estimated abundance of BFT obtained using detection function 1A. Black colours show estimates from this report: dots show estimated values for each year of surveys and thin lines indicate upper and lower limits of the 95% confidence interval. Orange colour shows estimates from Chudzinska et al. (2024).

5.2.3 Estimated biomass for years 2017-2024

The biomass estimates are presented in Table 6 and Figure 7. The estimates for the previous years based on the newest detection function are comparable with the estimates from the previous reports; deviations in blocks C and E are likely due to the slight change in the company factor. There is a decrease in biomass in all blocks compared to 2023 (Figure 7).

Table 6. Estimated biomass (B, in tonnes) per block and year with coefficient of variation (CV) and lower (LCL) and upper (UCL) 95% confidence levels. Coefficient of variation (CV) is also provided for the results from this analysis. The orange values apply to estimates reported in Chudzinska et al. (2024). All estimates are based on sightings from all blocks: A, C, E and G.

Block-Year	B	CV	LCI	UCI	B	CV	LCI	UCI
	This report				Chudzinska et al. (2024)			
A-2017	9300	0.4	4020	21513	8726	0.44	3774	20177
A-2018	15569	0.3	8591	28212	14603	0.31	8034	26544
A-2019	13797	0.4	6407	29713	12948	0.40	6015	27871
A-2021	5325	0.5	1950	14539	5183	0.53	1905	14105
A-2022	10375	0.5	4358	24702	10640	0.46	4441	25493
A-2023	10597	0.5	4184	26842	10970	0.49	4289	28056
A-2024	2200	0.8	5333	9078				
C-2017	7524	0.4	3390	16700	6994	0.40	3167	15442
C-2018	5622	0.6	1861	16981	5238	0.58	1740	15767
C-2019	3427	0.6	1123	10458	3186	0.58	1047	9696
C-2022	12254	0.4	5436	27621	10770	0.43	4677	24804

C-2023	4646	0.7	1310	16474	4054	0.68	1140	14412
C-2024	3907	0.7	1112	13730				
E-2017	7097	0.6	2382	21150	6393	0.58	2147	19040
E-2018	4157	0.6	1433	12061	3865	0.57	1335	11189
E-2019	2255	0.5	907	5604	2096	0.47	848	5176
E-2022	1029	0.8	244	4343	2110	0.76	537	8284
E-2023	17092	0.4	7325	39882	14954	0.44	6299	35500
E-2024	9771	0.6	3437	27781				

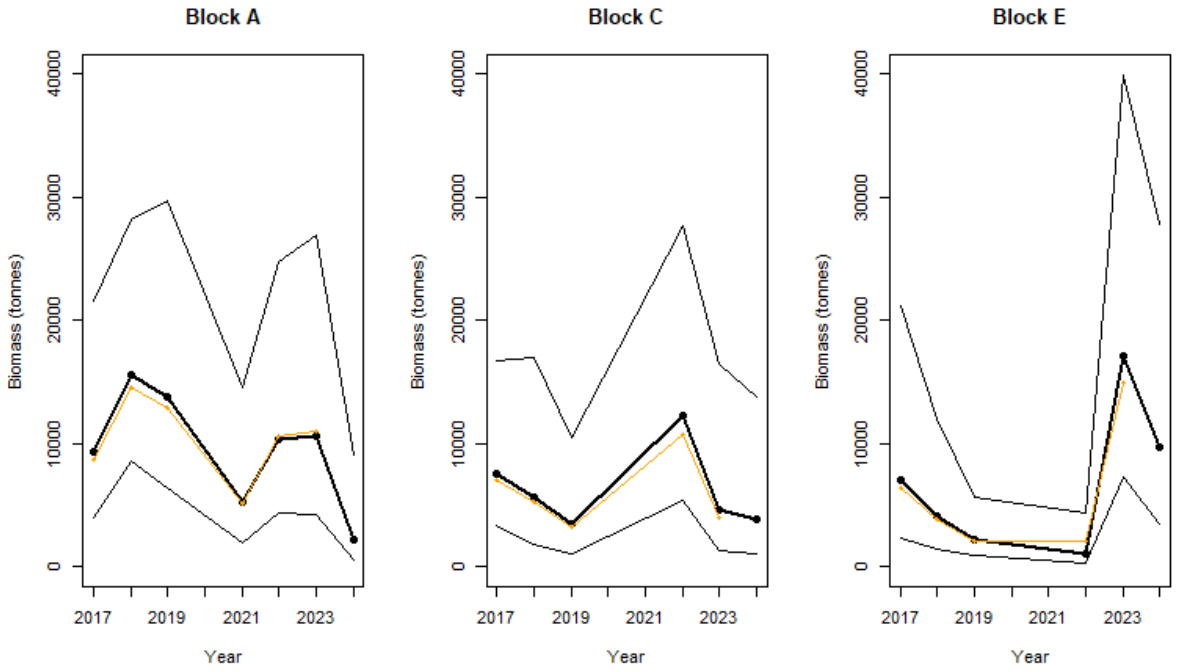

Figure 7. Estimated biomass (in tonnes) of BFT. Black colours show estimates from this study: dots show estimated values, and thin lines indicate upper and lower limits of the 95% confidence interval. Orange colour shows estimates from the Chudzinska et al. (2024).

5.3 Task 1 – revision of indices based on data from three blocks (A, C and E)

5.3.1 Detection function for abundance and biomass

Models tested are shown in Appendix B (Tables B3 and B4) and the resulting models are like those fitted previously, including detections in block G. For the abundance detection function (1C), *log(size)* and *company* was selected. The best model for biomass (1D) was *log(biomass)* and *company*.

The histograms of detections in Figure 8 are like those in Figure 5.

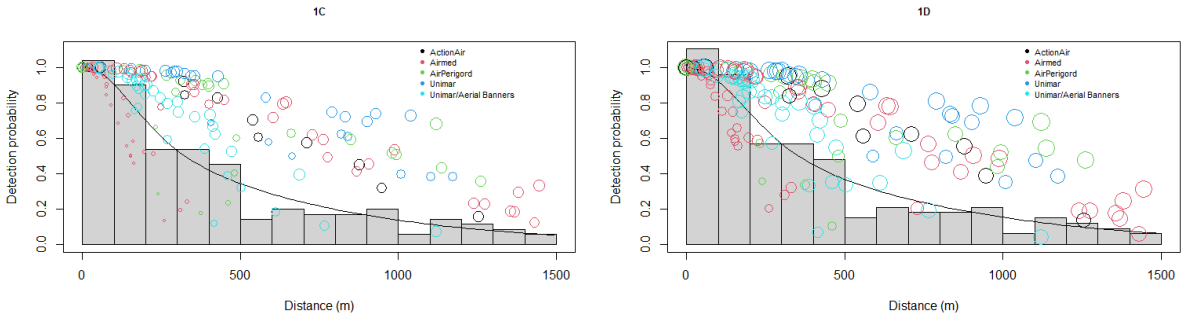

Figure 8. Detection functions 1C (abundance) and 1D (biomass): histogram of observed distances, detection function averaged across all observations (black line) and detection probabilities of observed distances and sizes/biomass (dots). Size of dots are scaled to represent the logarithm of school size (1C) and logarithm of biomass (1D).

5.3.2 Estimated abundance for years 2017-2024

Estimated abundances are given in Table 7. For all blocks there is a decrease in estimated abundance in comparison with estimates from 2023. After a peak in 2022, block C estimates in 2023 and 2024 are like those in 2017 to 2019. Figure 9 shows the comparison between current estimates and estimates of the abundance from the previous report; the current results are comparable with previous estimates.

Table 7. Estimated number of individual tuna (N, in thousands) per block and year with coefficient of variation (CV) and lower (LCL) and upper (UCL) 95% confidence levels. Coefficient of variation (CV) is also provided for the results from this analysis. The orange values are from Chudzinska et al. (2024). All estimates are based on sightings from all blocks: A, C and E.

Label	N	CV	LCI	UCI	N	CV	LCI	UCI
	This report				Chudzinska et al. (2024)			
A-2017	53.2	0.4	23.5	120.4	50.3	0.4	22.2	114.0
A-2018	87.0	0.3	48.6	155.7	82.2	0.3	45.7	147.7
A-2019	82.1	0.4	38.4	175.6	77.7	0.4	36.3	166.4
A-2021	44.8	0.6	15.7	127.5	44.5	0.6	15.6	126.8
A-2022	62.8	0.4	26.9	146.2	38.6	0.4	18.5	80.8
A-2023	58.4	0.5	23.7	144.2	58.6	0.5	23.7	144.6
A-2024	11.1	0.7	3.2	38.7				
C-2017	47.8	0.4	21.4	106.5	44.9	0.4	20.2	99.9
C-2018	39.6	0.6	13.3	118.3	37.4	0.6	12.6	111.2
C-2019	27.6	0.6	9.1	83.6	26.0	0.6	8.6	78.5
C-2022	176.8	0.4	81.6	283.3	157.1	0.4	70.6	349.5
C-2023	37.0	0.7	10.7	127.7	33.0	0.7	9.5	114.8
C-2024	30.7	0.7	8.9	105.9				
E-2017	48.7	0.5	18.3	129.6	44.2	0.5	16.6	117.9
E-2018	42.5	0.6	14.2	126.5	39.9	0.6	13.4	118.8
E-2019	32.2	0.5	12.6	82.7	31.1	0.5	12.1	79.9

E-2022	22.8	0.8	5.2	99.0	45.6	0.8	11.3	184.2
E-2023	166.4	0.4	76.7	360.9	148.7	0.4	66.7	331.5
E-2024	104.5	0.4	44.1	247.8				

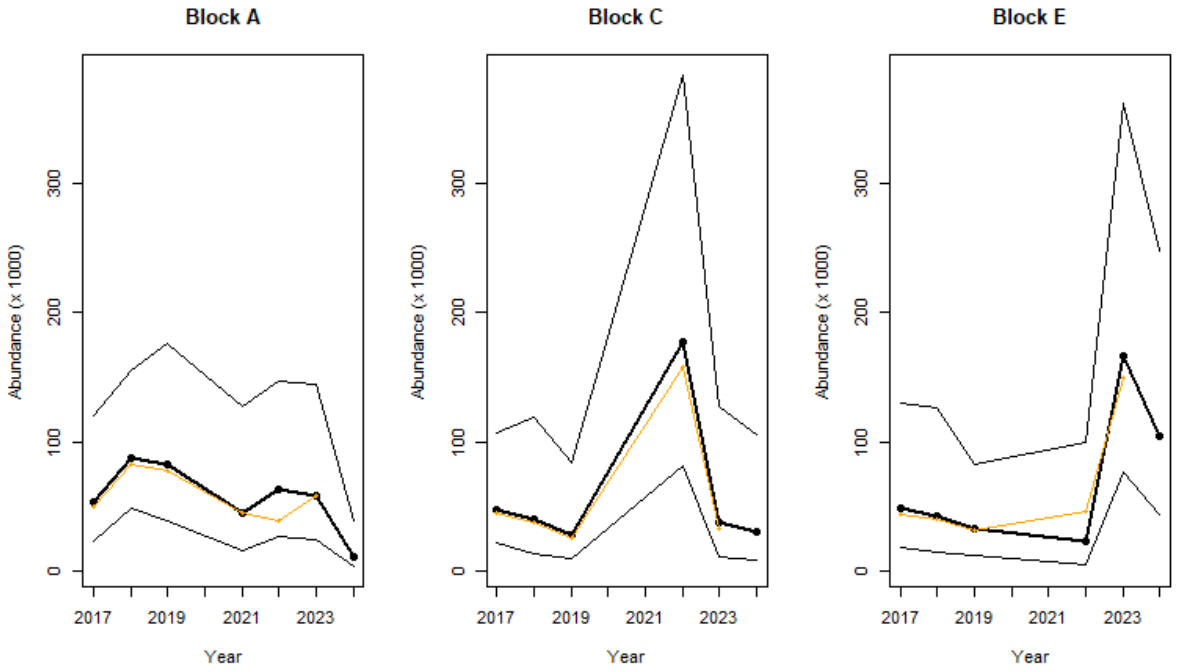

Figure 9. Estimated abundance of BFT obtained using detection function 1C. Black colours show estimates from this report: dots show estimated values for each year of surveys and thin lines indicate upper and lower limits of the 95% confidence interval. Orange colour shows estimates from Chudzinska et al. (2024).

5.3.3 Estimated biomass for years 2017-2023

The biomass estimates are presented in Table 8 and Figure 10. There is a reduction in biomass in all blocks compared to 2023. The estimates for the previous years based on the newest detection function are comparable with the estimates from the previous reports (Figure 10).

Table 8. Estimated biomass (B, in tonnes) per block and year with coefficient of variation (CV) and lower (LCL) and upper (UCL) 95% confidence levels. Coefficient of variation (CV) is also provided for the results from this analysis. The orange values apply to estimates in Chudzinska et al. (2024). All estimates are based on sightings from blocks: A, C and E.

Label	B	CV	LCI	UCI	B	CV	LCI	UCI
	This report				Chudzinska et al. (2024)			
A-2017	9223	0.4	3988	21331	8665	0.4	3747	20037
A-2018	15442	0.3	8520	27986	14499	0.3	7974	26364
A-2019	13683	0.4	6355	29460	12858	0.4	5973	27678
A-2021	7471	0.6	2663	20960	7287	0.5	2605	20387
A-2022	10259	0.4	4313	24403	10554	0.5	4408	25272
A-2023	10472	0.5	4139	26497	10877	0.5	4256	27799
A-2024	2175	0.8	528	8969				
C-2017	7487	0.4	3376	16606	6970	0.4	3158	15382

C-2018	5597	0.6	1854	16896	5221	0.6	1735	15712
C-2019	3411	0.6	1118	10403	3175	0.6	1044	9661
C-2022	12188	0.4	5410	27456	10735	0.4	4663	24718
C-2023	4613	0.7	1303	16333	4036	0.7	1136	14337
C-2024	3880	0.7	1105	13627				
E-2017	7036	0.6	2361	20962	6348	0.6	2131	18904
E-2018	4137	0.6	1426	12000	3852	0.6	1331	11147
E-2019	3553	0.5	1377	9165	3383	0.5	1313	8713
E-2022	1031	0.8	244	4348	2115	0.8	539	8301
E-2023	16987	0.4	7285	39613	14897	0.4	6277	35354
E-2024	9701	0.6	3417	27539				

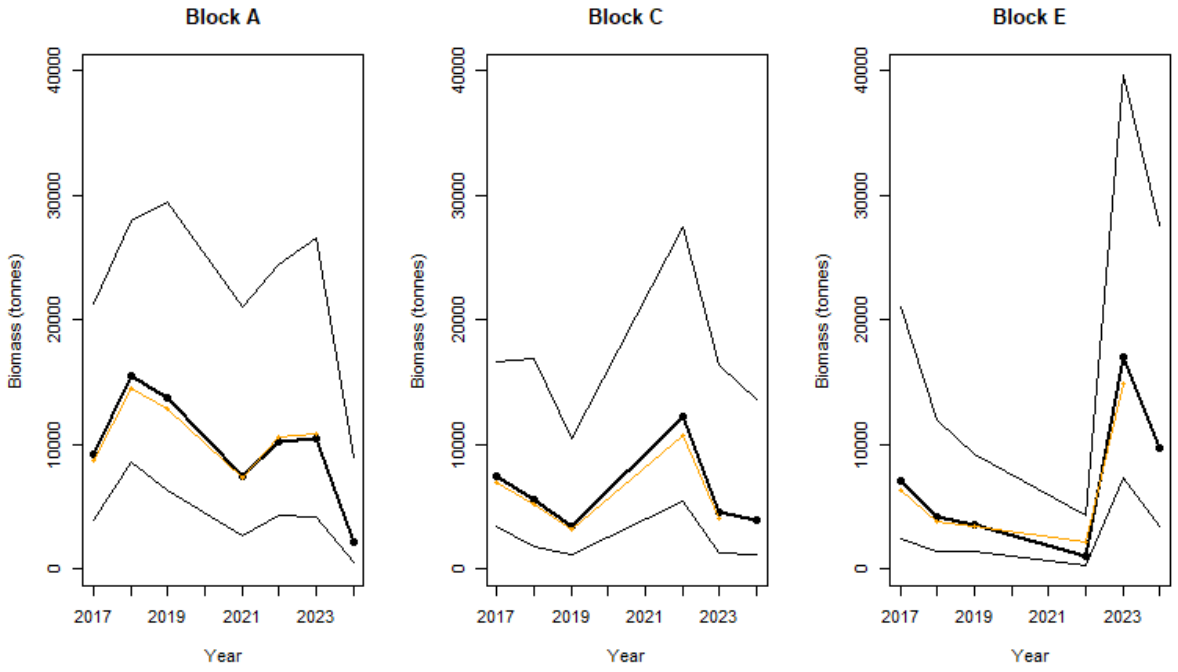

Figure 10. Estimated biomass (in tonnes) of BFT. Black colours show estimates from this study: dots show estimated values, and thin lines indicate upper and lower limits of the 95% confidence interval. Orange colour shows estimates from the Chudzinska et al. (2024).

5.3.4 Comparison between detections function including/excluding block G

The detection functions based on all four blocks (A, C, E and G) are based on 182 detected groups. Excluding area G leads to the reduction in the number of groups to 170. Comparison of the average probability of detection and uncertainty around this parameter shows that excluding area G slightly decreases the average probability of detection (Table 9).

Table 9. Comparison of the estimated probability of detection (*p*), averaged over all detections, for the detection functions fitted to the data from 2017 to 2024.

Detection function	Data used	Average p estimate	Average p CV

1A	A,C,E,G – school size	0.33	0.10
1C	A,C,E – school size	0.32	0.09
1B	A,C,E,G - biomass	0.35	0.09
1D	A,C,E - biomass	0.34	0.09

5.3.5 Task 2 – strict update

The results for 2024 assuming an identical function to that fitted in Paxton et al. (2023) are given in Table 10. For block A the point estimates are very similar to those from Task 1A (Table). For blocks C and E, the estimates are different although there is substantial overlap in confidence intervals of the two estimates despite the change in factor levels.

Table 10. Estimated number of individuals (N, in thousands) and biomass (tonnes) per block in 2024 with lower (LCL) and upper (UCL) limits for a 95% confidence interval. Coefficient of variation (CV) is also provided for the results from this analysis. All estimates are based on detections from all blocks: A, C, E and G from 2017 to 2022.

Label	N	CV	LCI	UCI	B	CV	LCI	UCI
	Abundance				Biomass			
A-2023	47.0	0.5	18.6	118.5	9420	0.5	3772	23523
C-2023	34.8	0.7	10.2	119.3	3714	0.7	1066	12937
E-2023	157.3	0.4	72.4	341.4	13752	0.4	5972	31667
A-2024	8.5	0.7	2.4	30.5	1979	0.8	487	8046
C-2024	29.1	0.7	8.5	99.8	3115	0.7	897	10816
E-2024	98.5	0.4	41.6	232.9	7868	0.5	2839	21806

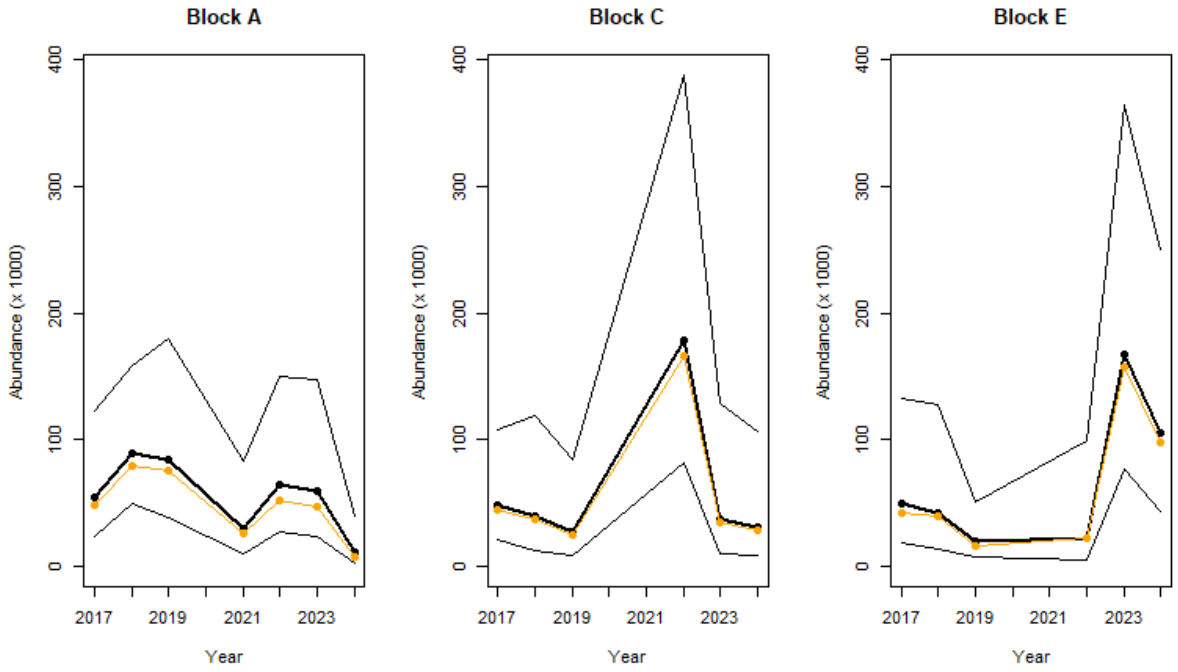

Figure 11. Estimated abundance (in thousands) of BFT for surveyed years and blocks. Black colours show estimates based on all four blocks (A, C, E and G) for Task 1 (detection function 1A): dots show estimated values and thin lines show upper and lower limits of the 95% confidence interval. Orange colour shows estimates based in Task 2.

The biomass results are very similar to the pattern in the abundance estimates for all three blocks and to estimates from Task 1A (Table).

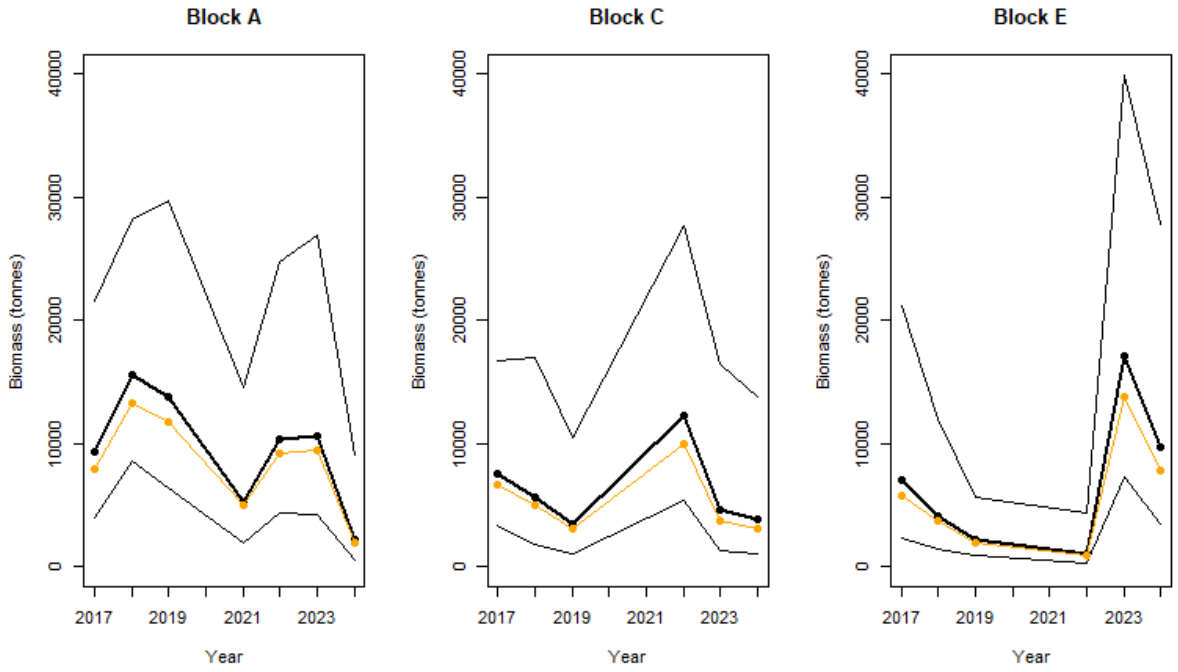

Figure 17. Estimated biomass (in tonnes) of BFT for surveyed years and blocks. Black colours show estimates based on all four blocks (A, C, E and G) for Task 1 (based on detection function 1A): dots show estimates and thin lines indicate upper and lower limits of the 95% confidence interval. Orange colour shows estimates obtained in Task 2.

6 Discussion

It should be stressed that the estimates given here are based on detections of fish observed at the surface, or close enough to the surface to be detected and that fish available to be detected on the transect (i.e. at zero distance) are certain to be detected. Hence these estimates provide indices of relative abundance and biomass rather than absolute numbers/biomass. This may be different to the absolute number/biomass of fish because neither the availability of fish to be detected nor the detection of available fish on the transect have been considered.

The analysis presented in Task 1 revealed that there is little difference between the abundance and biomass estimates between analysis based on all four blocks (A, C, E and G) and just three blocks (A, C, E) and both estimates are well within the confidence intervals of each other. Estimates are not provided for block G but including these data in the detection function is consistent with the biomass and abundance estimates of the ICCAT GBYP programme and useful in case block G is surveyed again in the future.

Task 1 calculated four detection functions: based on the size of the detected schools including and excluding sightings from area G; and based on biomass of the detected schools including and excluding sightings from area G. All selected detection functions included the natural logarithm of the size/biomass of the detected schools and company. To be consistent with previous analyses, the five levels for company have been used but it may that the levels could be reduced; “Unimar” and “Unimar/Aerial Banners” seem to provide a service in collaboration and so could be combined into one level.

While adding new data (here, new surveyed year) and calculating a new detection function based on additional data, estimates and confidence intervals for the previous years can be updated. The approach used in Task 2 does not allow for such updates as the calculation is based on detection function on a reduced data set (i.e. not including sightings from 2023 or 2024).

7 Acknowledgements

This work has been carried out under the ICCAT Atlantic-Wide Research Programme for BFT (GBYP), which is funded by the European Union, several ICCAT CPCs, the ICCAT Secretariat, and other entities (see https://www.iccat.int/gbyp/en/overview.asp). The content of this paper does not necessarily reflect ICCAT’s point of view or that of any of the other sponsors, who carry no responsibility. In addition, it does not indicate the Commission’s future policy in this area.

8 References

Akaike, H. 1987. Factor analysis and AIC. Pages 317-332 Psychometrika.

Buckland, S. T., D. R. Anderson, K. P. Burnham, J. L. Laake, D. L. Borchers, and L. Thomas. 2001. Introduction to Distance Sampling. Estimating abundance of biological populations. Oxford University Press, Oxford.

Chudzinska, M., L. Burt, D. Borchers, D. Miller, and S. Buckland. 2021. Design-based inference to estimate density, abundance and biomass of bluefin tuna. Reanalysis of 2010-2019 Aerial Surveys. Report number CREEM-2021-03. Provided to ICCAT, September 2021 (Unpublished).

Chudzinska, M., L. Burt, and S. Buckland. 2022. Design-based inference to estimate density, abundance and biomass of bluefin tuna. reanysis of 2017-2021 Aerial urveys of Region A. Report number CREEM-2022-03. Provided to ICCAT, July 2022 (Unpublished).

Chudzinska, M., C. G. M Paxton and L. Burt. 2024. Design-based inference to estimate density, abundance and biomass of bluefin tuna in the Mediterranean Sea. Analysis including the of 2023 aerial visual surveys. Report number CREEM-2024-03. Provided to ICCAT, April 2024 (Unpublished).

Laake, J., D. Borchers, L. Thomas, D. Miller, and J. Bishop. 2022. mrds: mark–recapture distance sampling. R package version 2.2.8. https://cran.r-project.org/package=mrds.

Marques, T. A., L. Thomas, S. G. Fancy, and S. T. Buckland. 2007. Improving estimates of bird density using multiple-covariate distance sampling. The Auk 124:1229-1243.

Miller, D. L., E. Rexstad, L. Thomas, L. Marshall, and J. L. Laake. 2019. Distance Sampling in R. Journal of Statistical Software 89:1 - 28.

Paxton, C. G. M., C. S. Oedekoven, M. Chudzinska, M. Pilar Tugores Ferrá, and D. Alvarez-Berastegui. 2023. Design- and model-based inference to estimate density, abundance and distribution of BFT in the Mediterranean Sea. Report number CREEM-2023-04. Provided to ICCAT, July 2023 (Unpublished).

Popov, D. and P. Feron. 2024. Aerial survey for the monitoring of Bluefin Tuna spawning aggregations in the Mediterranean Sea ICCAT GBYP Phase 14 Balearic Sea – Area A. Report to ICCAT.

R Core Team. 2024. R: A Language and Environment for Statisical Computing. R Foundation for Statistical Computing.

Unimar and AerialBanners. 2024a. Aerial survey for the monitoring of bluefin tuna spawning aggregations in the Mediterranean Sea. Call for tenders 04/2024 (ICCAT GBYP - Phase 14) - Circular # G-00262/2024 - Area C.

Unimar and AerialBanners. 2024b. Aerial survey for the monitoring of bluefin tuna spawning aggregations in the Mediterranean Sea. Call for tenders 04/2024 (ICCAT GBYP - Phase 14) - Circular # G-00262/2024 - Area E.

9 Appendix A: Summary of the survey blocks surveyed in each year

Table A1. Size of survey blocks and company and aircraft used to undertake the surveys and data used in the analysis: *k* is the number of transects, *L* is the total length of search effort and *n* is the number of detected adult groups within 1,500 m of the transects.

Year	Block	Area (km^2)	Company	Aircraft	k	L (km)	n
2017	A	61,837	Airmed	Partenavia	52	4996	18
	C	53,868	Unimar	Partenavia	25	4830	7
	E	93,614	Airmed	Partenavia	41	6382	4
	G	38,788	ActionAir	Cessna	57	3909	3
2018	A	61,837	Airmed	Partenavia	62	6154	24
	C	53,868	Unimar	Partenavia	25	4930	7
	E	93,614	Unimar	Partenavia	47	8821	7
	G	38,788	ActionAir	Cessna	56	4141	5
2019	A	61,837	Airmed	Partenavia	50	5460	19
	C	53,868	Unimar	Partenavia	23	4818	4
	E	93,614	ActionAir	Cessna	48	8332	6
	G	38,788	ActionAir	Cessna	53	5871	4
2021	A	61,837	ActionAir	Cessna	46	6264	7
2022	A	61,837	Air Perigord	Cessna	30	5367	9
	C	53,868	Unimar/Aerial Banners	Partenavia	25	4937	11
	E	93,614	Unimar/Aerial Banners	Partenavia	30	6541	3
2023	A	61,837	Air Perigord	Cessna	29	5277	14
	C	53,868	Unimar/Aerial Banners	Partenavia	25	5015	3
	E	93,614	Unimar/Aerial Banners	Partenavia	21	5181	8
2024	A	61,837	Air Perigord	Cessna	30	5688	7
	C	53,868	Unimar/Aerial Banners	Partenavia	25	4988	3
	E	93,614	Unimar/Aerial Banners	Partenavia	34	7234	8

Note that data from the survey block AO (an area surrounding block A) surveyed in 2021 were not included in this report and estimates are not provided for block G.

10 Appendix B: Model selection and goodness-of-fit

This appendix contains the AIC values for the fitted models (Tables B1-B4) and the goodness of fit statistics (Table B5 and Figure B1).

In Tables B1-B4, the AIC and ΔAIC (the difference between the AIC and the minimum AIC) for fitted models are provided. The key functions are half-normal (HN) and hazard rate (HR). A null model indicates that perpendicular distance was the only explanatory variable included in the detection function. The model in bold font indicates the selected model.

Table B1. Detection function 1A (including blocks A, C, E and G and school size).

Model	Key	AIC	ΔAIC
Log(size) + block	**HN**	**2496.00**	**0.00**
Log(size) + plane	HN	2505.79	9.80
Log(size) + company	HN	2507.93	11.94
Log(size)	HN	2508.41	12.42
Log(size) + block	HR	2513.58	17.59
Log(size) + plane	HR	2518.65	22.67
Log(size) + company	HR	2518.67	22.68
Log(size)	HR	2525.59	29.60
Company	HR	2532.59	36.60
Block	HR	2538.53	42.53
Plane	HR	2543.00	47.01
Null	HR	2546.58	50.59
Null	HN	2556.82	60.83
Plane	HN	2560.47	64.48
Company	HN	2561.83	65.84
Block	HN	2565.23	69.24
Year	HN	2666.01	170.02
Year	HR	2668.01	172.02
Log(size) + year	HN	2668.01	172.02

Table B2. Detection function 1B (including blocks A, C, E and G and biomass).

Model	Key	AIC	ΔAIC
Log(biomass) + company	**HN**	**2507.92**	**0.00**
Log(biomass) + company	HR	2517.00	9.08
Log(biomass) + plane	HN	2518.59	10.67
Log(biomass) + block	HR	2523.28	15.36
Log(biomass)	HN	2530.01	22.09
Company	HR	2532.59	24.67
Log(biomass)	HR	2533.65	25.73
Block	HR	2538.52	30.60
Plane	HR	2543.00	35.08
Null	HR	2546.58	38.66

Company	HN	2556.82	48.90
Null	HN	2560.47	52.55
Plane	HN	2561.83	53.91
Block	HN	2565.23	57.31
Year	HN	2666.01	158.09
Year	HR	2668.01	160.09
Log(biomass) + year	HN	2668.01	160.09
Log(biomass) + plane	HR	2670.01	162.09

Table B3. Detection function 1C (including blocks A, C and E and school size).

Model	Key	AIC	ΔAIC
Log(size) + company	**HN**	**2323.00**	**0.00**
Log(size)	HN	2332.70	9.70
Log(size) + company	HN	2333.71	10.72
Log(size) + plane	HN	2333.83	10.83
Log(size)	HR	2343.04	20.04
Log(size) + plane	HR	2343.35	20.36
Log(size) + block	HR	2346.60	23.60
company	HR	2361.00	37.97
Block	HR	2364.08	41.08
Null	HR	2369.63	46.63
Plane	HR	2369.97	46.97
Company	HN	2385.59	62.60
Null	HN	2388.77	65.78
Plane	HN	2390.46	67.46
Block	HN	2392.01	69.02
Year	HN	2490.50	167.50
Year	HR	2492.50	169.50
Log(size) + year	HN	2492.50	169.50

Table B4. Detection function 1D (including blocks A, C and E and biomass).

Model	Key	AIC	ΔAIC
Log(biomass) + company	**HN**	**2334.93**	**0.00**
Log(biomass)	HN	2340.17	5.24
Log(biomass) + plane	HN	2340.41	5.48
Log(biomass) + block	HN	2343.68	8.74
Log(biomass) + company	HR	2344.32	9.39
Log(biomass)	HR	2347.76	12.83
Log(biomass) + plane	HR	2348.30	13.37
Log(biomass) + block	HR	2350.50	15.56

Company	HR	2361.00	26.03
Block	HR	2364.08	29.15
Null	HR	2369.63	34.70
Plane	HR	2369.97	35.03
Company	HN	2385.59	50.66
Null	HN	2388.77	53.84
Plane	HN	2390.46	55.52
Block	HN	2492.01	57.08
Year	HN	2490.50	155.56
Year	HR	2492.50	157.56
Log(biomass) + year	HN	2492.50	157.56

Table B5. Goodness of fit statistic (Cramer-von Mises test) and associated *p*-value for the selected detection functions. None of the test statistics indicated a lack of fit, testing at the 5% significance level.

Detection function	Test statistic	*p*-value
1A	0.08	0.67
1B	0.17	0.33
1C	0.13	0.47
1D	0.23	0.22

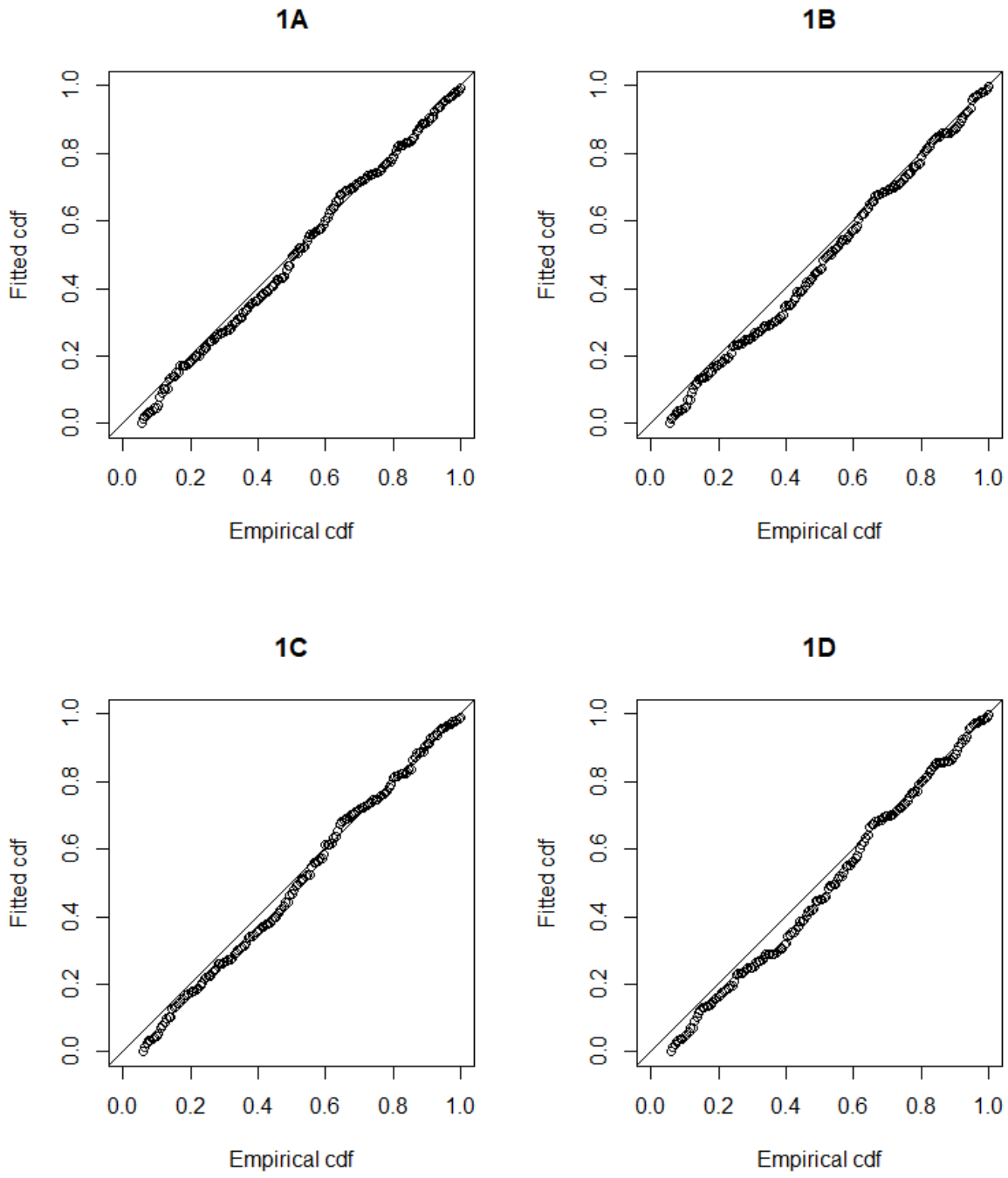

Figure B1. Q-Q plots for selected detection functions showing the observed (empirical) cumulative distribution function (cdf) against the fitted CDF with a line of equality. For good fitting models, the points should lie on the line of equality.